BIOCHEMISTRY
including biophysical chemistry & molecular biology

Article

pubs.acs.org/biochemistry

Expression, Purification, and Solid-State NMR Characterization of the Membrane Binding Heme Protein Nitrophorin 7 in Two Electronic Spin States

Sabu Varghese,[†,‡] Fei Yang,[§,⊥] Victor Pacheco,[†,‡] Kathrin Wrede,[∥] Alexander Medvedev,[‡] Hideaki Ogata,[∥] Markus Knipp,*[,∥,#] and Henrike Heise*[,†,‡]

[†]ICS-6 Institute of Complex Systems—Structural Biochemistry, Forschungszentrum Jülich, D-2425 Jülich, Germany
[‡]Institute of Physical Biology, Heinrich-Heine-Universität Düsseldorf, Universitätsstraße 1, 40225 Düsseldorf, Germany
[§]Department of Chemistry and Biochemistry, Miami University, Oxford, Ohio 45056, United States
[⊥]Department of Chemistry and Biochemistry, University of Arizona, Tucson, Arizona 85721, United States
[∥]Max-Planck-Institut für Chemische Energiekonversion, Stiftstrasse 34-36, 45470 Mülheim an der Ruhr, Germany
[#]Fakultät für Chemie und Biochemie, Ruhr-Universität Bochum, Universitätsstraße 150, 44801 Bochum, Germany

Supporting Information

ABSTRACT: The nitrophorins (NPs) comprise a group of NO transporting ferriheme *b* proteins found in the saliva of the blood sucking insect *Rhodnius prolixus*. In contrast to other nitrophorins (NP1−4), the recently identified membrane binding isoform NP7 tends to form oligomers and precipitates at higher concentrations in solution. Hence, solid-state NMR (ssNMR) was employed as an alternative method to gain structural insights on the precipitated protein. We report the expression and purification of ^{13}C,^{15}N isotopically labeled protein together with the first ssNMR characterization of NP7. Because the size of NP7 (21 kDa) still provides a challenge for ssNMR, the samples were reverse labeled with Lys and Val to reduce the number of crosspeaks in two-dimensional spectra. The two electronic spin states with $S = 1/2$ and $S = 0$ at the ferriheme iron were generated by the complexation with imidazole and NO, respectively. ssNMR spectra of both forms are well resolved, which allows for sequential resonance assignments of 22 residues. Importantly, the ssNMR spectra demonstrate that aggregation does not affect the protein fold. Comparison of the spectra of the two electronic spin states allows the determination of paramagnetically shifted cross peaks due to pseudocontact shifts, which assists the assignment of residues close to the heme center.

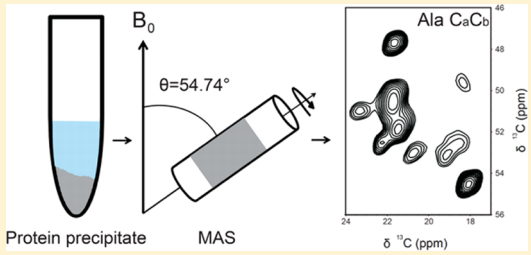

Nitrophorins represent a group of ferriheme *b* proteins designated NP1−4 and 7, which are found in the saliva of the blood-sucking insect *Rhodnius prolixus*.[1] The biological function of the NPs is the storage, transport, and delivery of NO from the insect saliva to the host tissue, where NO acts as a vasodilator and blood-coagulation inhibitor during feeding.[2,3] The radical NO (in vivo, $t_{1/2} \approx 100$ ms)[4] is preserved through coordination to the heme iron inside the insect saliva. The protein experiences a significant pH change and dilution when transported from the acidic pH of the saliva (between 5 and 6)[5] to that of the blood plasma (~7.4). Consequently, the affinity for NO is decreased, so that NO release occurs in the host tissue. In NPs, the heme cofactor is located inside an eight-stranded β-barrel.[6] The protein fold has been classified as a lipocalin type, which is a common fold within the proteome, especially for proteins that bind lipophilic molecules. The heme iron is coordinated by a proximal His residue and the sixth coordination site is open for coordination of various small ligands, including NO.[7]

In contrast to NP1−4, NP7 contains a high number of positively charged Lys residues,[8] which results in the high pI of 9.2 compared to 6.1−6.5 for NP1−4.[9] The majority of the Lys residues cluster at the protein's surface opposite to the opening to the heme pocket and can thus attach to negatively charged phospholipid membranes.[8,10,11] Due to its bipolar charge distribution, NP7 tends to form oligomers and insoluble aggregates in solution.[12−17] Therefore, solution-state NMR studies of NP7 were hampered by broad resonances due to slow molecular tumbling rates of transient aggregates and thus accelerated T_2 relaxation.[18] Recently, crystallization conditions for NP7 were established that yield small crystals;[19] however, certain ill-defined electron density in the heme pocket complicates the refinement process. To gain insight into the structural features of NP7, solid-state NMR (ssNMR) spec-

Received: July 28, 2013
Revised: September 11, 2013
Published: September 13, 2013

troscopy of NP7 was used as a viable alternative to elucidate the structure.

Despite the recent advancement and success of ssNMR in solving the three-dimensional structures of complex biomolecular systems,[20] determination of high quality atomic-resolution protein structures using ssNMR is an ongoing challenge due to the relative scarcity of unambiguous long-range distance restraints. The presence of intrinsic or extrinsic paramagnetic centers can be of immense help to obtain structural restraints because their intrinsic magnetic field leads to significant alterations of the chemical shifts of nuclei in close proximity (Fermi contact shifts, pseudocontact shifts (PCS)) and because of the paramagnetic relaxation enhancement (PRE) that is thoroughly described elsewhere.[21−23]

The successful use of PCSs in ssNMR has been demonstrated for studying the structural changes involving an amino acid residue (Phe87) of a 119 kDa paramagnetic enzyme (cytochrome P450 BM-3) upon substrate (*N*-palmitoylglycine) binding using selective labeling and relaxation filters.[24,25] Bertini et al. have exploited PCSs for structure determination of microcrystalline Co^{II}-substituted matrix metalloproteinase 12 (Co^{II}MMP-12).[26−29] Furthermore, determination of structure and dynamics of the relatively large metalloenzyme Cu/Zn superoxide dismutase (SOD, 32 kDa in the dimeric form) has recently been reported using an extensive set of ^{15}N and ^{13}C nuclear relaxation rates with ^{1}H detection under ultrafast magic-angle spinning (MAS).[30]

Here we report initial ssNMR studies of NP7 in the Fe^{III} low-spin (LS) state ($S = 1/2$) and the diamagnetic ($S = 0$) NO bound form (i.e., $\{FeNO\}^6$ in the notation of Enemark and Feltham).[31] Although the tendency of the protein to oligomerize prevents studies by solution NMR spectroscopy, we took advantage of the protein's intrinsic propensity to aggregate and investigated protein precipitated from concentrated solution.

MATERIALS AND METHODS

Protein Expression and Purification. Prior to recombinant expression, $pNP7^{Kan}$ was transformed into *Escherichia coli* strain BL21 (DE3) (Novagen). Natural abundance NP7 was expressed in LB medium (1% (w/v) tryptone, 0.5% (w/v) yeast extract, and 1% (w/v) NaCl) at 37 °C as described previously.[10] The medium was supplemented with 30 mg L^{-1} kanamycin A and 0.005% (v/v) Antifoam 204 (Sigma Aldrich).

For the expression of labeled protein, an overnight culture of 1 L was set up for growth at 37 °C. For the expression culture, a minimal medium was prepared of the following composition: 6 g L^{-1} NaH_2PO_4, 3 g L^{-1} K_2HPO_4, 0.5 g L^{-1} NaCl, 8 mM $MgSO_4$, 0.8 mM $CaCl_2$, 2 g L^{-1} [U-$^{13}C_6$]-D-glucose, and 1 g L^{-1} $^{15}NH_4Cl$. The pH of this solution was titrated with KOH to pH 7.5. One liter of this solution was further supplemented with 10 mL of trace element solution, 1 mL 100 × BME vitamins (Sigma Aldrich), 50 μL of Antifoam 204 (Sigma Aldrich), 1 mL of 10% (w/v) yeast extract, 5 mg of $(NH_4)_2Fe(SO_4)_2{\cdot}7H_2O$, and 1 mL of 30 mg L^{-1} kanamycine A. One liter of the trace element solution contained 5 g of Na_2EDTA, 4 mg of Na_2MoO_4, 50 mg of $ZnCl_2$, 10 mg of $CuCl_2$, 10 mg of $CoCl_2{\cdot}6H_2O$, 10 mg of H_3BO_3, and 400 mg of $MnCl_2{\cdot}4H_2O$. The overnight culture was centrifuged, and the cells were resuspended in 0.9% (w/v) NaCl. Afterward, 2 L of the expression culture was inoculated with the cells of the overnight culture, and expression was immediately induced with 1 mM of isopropyl-β-D-thiogalactopyranosid (IPTG). In the case of the reverse labeled sample (see below), 100 mg L^{-1} each of L-lysine and L-valine were added.

The expression was performed on a shaker at 37 °C. After the cells were harvested, they were broken using an Emulsiflex C-15 high pressure homogenizer (Aventis) with a pressure of 1500 bar. The protein was yielded as inclusion bodies, which were washed and solubilized in 6 M guanidinium chloride (GndCl). Subsequently, the protein was refolded and reconstituted with the heme cofactor essentially as described previously.[10] Upon size exclusion chromatography (SEC), a novel chromatographic step using Chelating Sepharose was introduced.

Chelating Sepharose Chromatography. A 5 mL HiTrap Chelating Sepharose column (GE Healthcare) was at first loaded with 100 mM $CaCl_2$ in 1% (v/v) CH_3COOH. Afterward, the column was equilibrated with 50 mM MOPS/NaOH (pH 6.8), 2% (v/v) glycerol. Combined fractions from SEC were then bound to the column. Elution was performed with a linear gradient of 0−40 mM $CaCl_2$. In another experiment, the column was not charged with Ca^{2+}, and elution was performed with a linear gradient of 0−40 mM L-glutamic acid. The elution profile was monitored by the absorbance at 280 nm absorption (Figure S1 of the Supporting Information), and fractions of 1 mL were collected.

Protein Characterization. After preparation, the protein is routinely characterized by UV−vis spectroscopy, SDS−PAGE (Figure S2 of the Supporting Information), and matrix-assisted laser desorption/ionization-time-of-flight (MALDI-TOF) mass spectrometry (Figure S3 of the Supporting Information) to be >95% pure. Prior to mass spectrometry, samples were concentrated and depleted of buffer components using $ZipTip_{C18}$ (Millipore) according to the supplier's protocol. Samples were eluted with 2 μL of 0.1% trifluoroacetic acid (TFA), 75% CH_3CN, and spotted on sinapinic acid.

Solution NMR Sample Preparation and Relaxation Experiments (T_1 and T_2). NP7 samples in 100 mM NaOAc/HOAc (pH 5.0) were concentrated using Biomax ultrafiltration concentrators (NMWL: 10 kDa) (Millipore). The buffer was exchanged through extensive washing (>3 times) with 30 mM sodium phosphate/acetic acid-d_4 buffer in D_2O (pH* 5.0). *Wt* NP2 samples were prepared from lyophilizates, as has been previously described.[12,32] NMR samples finally consisted of 1−2 mM protein. To obtain the LS complexes, the high-spin (HS) samples were titrated with imidazole (ImH) until the proton NMR signals in the 70−30 ppm region, indicative of the HS form, had just disappeared. Concomitantly, these signals were replaced by much sharper signals in the 35−10 ppm region.

NMR T_1 and T_2 relaxation data were collected with the chemical shifts referenced to residual protonated water at 4.7 ppm on a Bruker DRX-600 spectrometer, operating at 600.13 MHz proton Larmor frequency equipped with a room temperature triple resonance probe (TXI). T_1 values were measured by the inversion−recovery method with presaturation of the solvent signal during the relaxation delay. T_2 values were measured by the Carr−Purcell−Meibohm−Gill (CPMG) method with presaturation during the relaxation delay. The peaks were integrated using Felix software (Felix NMR, Inc., Felix 2007). After each dilution, more ImH was added to reach the same ImH concentration.

Diffusion Ordered Spectroscopy (DOSY) Experiments. Solution-state DOSY measurements were performed on a Varian INOVA 600 MHz spectrometer operating at 599.644 MHz with a room temperature 5 mm probe head equipped

with three orthogonal gradient coils. ^{1}H (^{13}C) DOSY measurements were conducted using the standard Varian $^{1}H^{13}C$-DOSY-heteronuclear single quantum coherence (HSQC) pulse sequence without spinning and at 25 °C.[33,34] The gradient was calibrated at 25 °C with a deuterated methanol sample using diffusion values previously obtained by NMR, for CD_3OH ($D = 2.22 \times 10^{-9}$ m^2/s) and for CHD_2OD ($D = 2.18 \times 10^{-9}$ m^2/s).[35,36] The gradient strength was incremented in 25 steps from 11.1 to 59.3 G/cm. The diffusion time was 0.25 s with a gradient duration of 1000 μs. The water signal was suppressed using the WATERGATE sequence.[37] Measurements were performed with 0.25 mM of [U-^{13}C,^{15}N \(K,V)]NP7−NO in 30 mM KH_2PO_4/KOH (pH 5.0) with 10% D_2O. Ensemble average of the molecular masses of the phosphate anions (M_r = 96.98) was used as an internal reference for approximating the molecular weights of the different NP7 oligomeric complexes. Further details about the theoretical and practical aspects of the procedure are given elsewhere.[38,39]

Solid-State NMR Experiments. For the ssNMR experiments, the protein samples were concentrated in ultrafiltration spin concentrators (Amicon ultra 10 K, Millipore) where, as a final step, the buffer was exchanged to 30 mM KH_2PO_4/KOH, 2% (v/v) glycerol, and 1 mM glutathione disulfide (GSSG) (pH 5.0). The final concentrations reached approximately 2 mM. NO loaded samples were prepared by the addition of a small molar excess of diethylammonium (*Z*)-1-(*N*,*N*-diethylamino)diazenolate-2-oxide (DEA/NO) dissolved in 10 mM NaOH. ImH loaded samples were prepared by the addition of 10 mM from a solution of 1 M ImH/HCl (pH 5.0). Upon concentration the protein precipitated within half an hour into fine red aggregates (Figure S4 of the Supporting Information). Micrographs of the precipitates were obtained in transmitted light mode on a Leica AF 6000 LX microscope equipped with 100 × 1.47 oil and 10 × 0.30 dry objectives. The Hamamatsu C9100-02 EM-CCD camera was operated at an exposure time of 1 ms and an electron multiplying (EM) gain of 10. The protein aggregates were transferred by spatula and centrifuged down into a 3.2 mm diameter MAS rotor for the ssNMR experiments.

The ssNMR spectra were taken on a Varian VNMRS NMR spectrometer equipped with a 3.2 mm HXY BIOMAS probe tuned in the $^{1}H/^{13}C$ mode or $^{1}H/^{13}C/^{15}N$ triple resonance mode operating at a field strength of 14.1 T (600 MHz ^{1}H frequency). Spectra were recorded at MAS frequencies of 8, 11, and 15 kHz. Pulse sequences were implemented with linear-ramped cross-polarization (CP)[40] with small phase incremental alternation (SPINAL)[41] ^{1}H decoupling at ∼83.3 kHz. The typical $\pi/2$ pulse widths were 3 μs on ^{1}H and 6 μs on ^{13}C. All the two-dimensional (2D) data were processed using NMRPipe[42] with forward and backward linear prediction in the indirect dimension, zero filled, and apodized with a combination of an exponential and a Gaussian function (GMB) for both dimensions before Fourier transformation. Additional acquisition and processing parameters for each spectrum are provided in the figure captions. Chemical shifts were referenced externally to adamantane.[43] Temperature calibration was achieved using nickelocene as an external reference.[44] At a spinning rate of 11 kHz, the actual sample temperature was found to be 10−15 °C above the nominal temperature displayed by the variable temperature unit. In this publication, we always refer to the nominal temperature instead of the actual sample temperature. All multidimensional spectra were analyzed using Sparky version 3.115 (T. D. Goddard and D. G. Kneller, University of California, San Francisco).

RESULTS AND DISCUSSION

Protein Expression and Purification. The recombinant expression of ^{13}C and ^{15}N double labeled NP7 was performed in minimal medium supplemented with [U-$^{13}C_6$]-D-glucose and $^{15}NH_4Cl$. The yield of protein in the minimal medium was slightly lower compared to the LB medium (approximately 5 mg L^{-1}) indicating, however, that sufficient amounts of protein can be obtained. The successful incorporation of ^{13}C and ^{15}N into the protein was demonstrated by MALDI-TOF MS (Table S1 and Figure S3 of the Supporting Information). Recombinantly expressed NPs are typically prepared from inclusion bodies formed in the cytosol of *E. coli* cells. The low cytosolic reduction potential does not allow the formation of the two disulfide bonds that are required for the native protein structure. These disulfide bonds are, therefore, established during the protein preparation, and the heme cofactor is inserted after the formation of the native fold, which then allows the protein to host the heme cofactor.

Samples reversely labeled for Lys and Val (termed [U-^{13}C,^{15}N\(K,V)]NP7) were produced by adding in excess L-lysine and L-valine in natural abundance to the medium. Where the final yield of the protein was similar to that of the fully labeled protein, MALDI-TOF MS indicated the successful isotopic distribution (Table S1 and Figure S3 of the Supporting Information). The deviation of molecular mass by 63 Da in [U-^{13}C,^{15}N\(K,V)]NP7 from the expected value is probably due to isotopic scrambling between Val and Leu.[45,46] Likewise, de novo synthesis of the reversely labeled residues Lys and Val is not completely suppressed: in the insensitive nuclei enhanced by polarization transfer total through bond correlation spectroscopy (INEPT TOBSY) spectrum (Figure S5 of the Supporting Information), which displays only signals from mobile fractions or monomers. However, in the double-quantum spectrum, which displays only rigid parts of the sample, where the shift dispersions between different amino acids of the same type is larger, a complete side chain walk could not be established for the Lys and Leu residues (Figures S5 and S6 of the Supporting Information). Thus, addition of Lys and Val in natural abundance strongly suppresses, but does not completely prevent, de novo synthesis from glucose.

Further purification was achieved by an additional chromatographic step. Because of the strong basicity of NP7, cation exchange chromatography should be feasible. However, attempts to purify the protein on common cation exchange media resulted in the loss of protein due to denaturation. We ascribe this to the instability of the fold in high ionic strength, which is required for protein elution. A method was developed using Chelating Sepharose HP, which provides iminodiacetic acid groups for binding. The protein readily binds to the resin and can be eluted with glutamic acid. Glutamic acid is used as an eluent because it contains two carboxylates so that lower concentrations of eluent are required (i.e., less ionic strength). Furthermore, we knew from the purification protocol that glutamate stabilizes the protein.[10] The elution profile demonstrates that some contaminants are well separated from the protein (see Figure S1 of the Supporting Information).

Losses of NP7 could be further minimized by charging the column with Ca^{2+} prior to the protein binding step. When the protein is loaded onto the column, NP7 and Ca^{2+} supposedly compete for the resin carboxylates, which is indicated by a

dx.doi.org/10.1021/bi401020t | *Biochemistry* 2013, 52, 7031−7040

broader distribution of the red color at the top of the resin. Figure S1 (Supporting Information) shows an example where elution was performed with a linear gradient of $CaCl_2$ where essentially all of the applied protein was recovered. The elution profile indicates that the protein is well separated from impurities and is now ready to perform the NMR experiments, which are also confirmed by SDS−PAGE.

NP7 Oligomerizes in Solution. In previous solution NMR experiments of NP7, severe line broadening was observed compared to NP1−4.[9,18] It was assumed that this is an effect of aggregation at the high concentrations required for NMR measurements (1−2 mM). This assumption was strongly supported by dynamic light scattering (DLS) measurements on NP7, where the apparent hydrodynamic diameters of the oligomers were of the order of ∼250−400 Å, which corresponds to oligomers of approximately 6−10 units.[9]

To further test this assumption, the variation of T_1 and T_2 for NP7 as a function of concentration was explored. T_1 and T_2 have different functional dependencies on the average tumbling time τ_c, which is a measure for the average hydrodynamic radius of the protein or oligomer. Thus, the degree of oligomerization on the protein concentration can be estimated through the concentration dependence of T_1 and T_2. In the slow motion regime, T_1 should decrease while T_2 should increase with decreasing τ_c corresponding to a smaller oligomer size, as expected for lower protein concentrations. T_1 and T_2 were determined for NP7 at three different concentrations using inversion−recovery or the CPMG pulse sequences, respectively. For comparison, both relaxation times were also determined for NP2, which does not form oligomers. Longitudinal relaxation for NP7 could not be fitted to a monoexponential curve but appears to follow a biexponential magnetization build-up. However, it was not possible to quantitatively determine T_1 values at different concentrations (Figure S7 of the Supporting Information). In contrast, for NP2, the longitudinal relaxation could be fitted to a monoexponential curve. Transverse relaxation, however, decayed monoexponentially for NP7 at all concentrations. As expected for oligomer formation at higher concentrations, the T_2 value decreased significantly from 3.87 to 1.79 ms, as protein concentration was increased from 0.125 to 2 mM. In contrast, T_2 values for NP2 amount to over 5 ms and are thus significantly longer and almost independent of protein concentration. As a conclusion, the oligomerization appears to occur only in NP7 but not in NP2, as proposed before.[9] The concentration dependence of T_2 in the case of NP7 implies that the average molecular weight decreases as concentration decreases, which means that at concentrations that are biologically relevant (<0.1 mM) the protein exists mainly as a monomer. However, the very short T_2 times of NP7 resulted in drastic line broadening (leading to line widths of up to 200 Hz), and the full assignment of heme resonances in solution NMR is very difficult.

To more accurately determine the state of oligomerization, DOSY experiments on [U-^{13}C,^{15}N\(K,V)]NP7−NO in solution were recorded at 25 °C and at a ^{1}H Larmor frequency of 600 MHz (Figure S8b of the Supporting Information). The spread of signals in the DOSY plot indicates a mixture of NP7 oligomers. The diffusion coefficients obtained from the 2D plot were used for the calculation of molecular weights (Table S2 of the Supporting Information). T_2 can be short for slowly tumbling high molecular weight oligomeric assemblies, and this can lead to a severe loss of signal.[47] Therefore, oligomers with molecular weights in excess of 50 kDa are difficult to detect by standard pulsed field gradient (PFG) NMR methods using stimulated echoes.[47,48] For thermostable macromolecules, one simple solution to this problem is to increase the overall molecular tumbling rate by recording NMR spectra at elevated temperatures.[49,50] However, measurements at a higher temperature of 35 °C resulted in the irreversible precipitation of the protein in the NMR sample tube, which is in good agreement with the thermal instability observed before.[9]

NP7 Precipitates at High Concentrations. At concentrations required for NMR measurements (2 mM), the sample containing diamagnetic [U-^{13}C,^{15}N\(K,V)]NP7−NO was already completely precipitated (Figure S4 of the Supporting Information). The resulting precipitate could directly be transferred into MAS rotors. To test whether the precipitate contained residual monomers or if certain regions of the protein are undergoing high amplitude motions at a time scale $<10^{-6}$ s, we investigated the dynamics of the sample in more detail. We recorded dipolar-driven cross-polarization magic-angle spinning (CPMAS) spectra,[51] and refocused INEPT[52] (red) spectra [U-^{13}C,^{15}N\(K,V)]NP7−NO at different temperatures from −30 to +10 °C in steps of 20 °C (Figure 1).

To clarify whether the precipitates were immobilized by the formation of stable aggregates or by the formation of transient sediments by MAS,[53] both types of spectra were recorded without MAS and with MAS at 11 kHz. The freezing of the

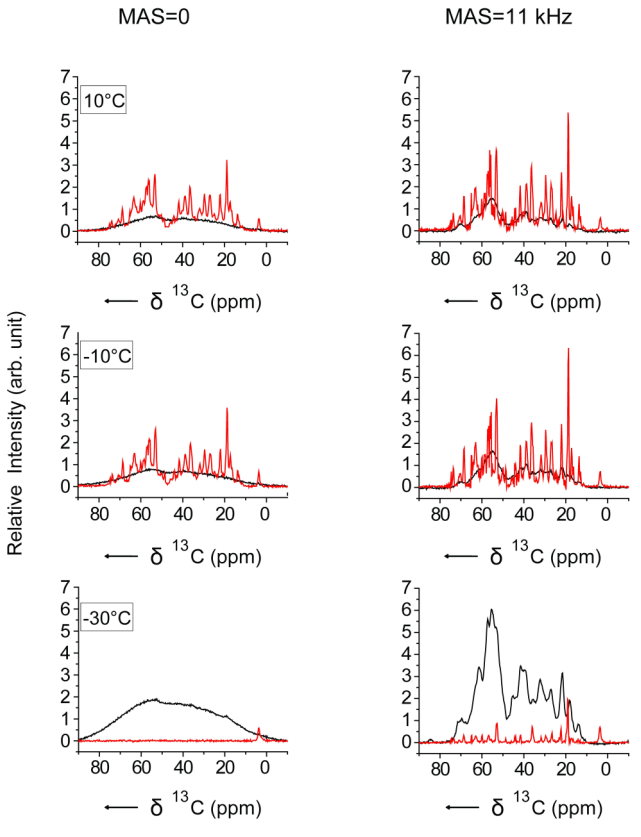

Figure 1. Temperature dependent 1D ^{13}C spectra of [U-^{13}C,^{15}N\(K,V)]NP7−NO in the diamagnetic state recorded using CP (black) and INEPT (red) based methods with and without MAS. All the spectra were recorded at a ^{1}H Larmor frequency of 600 MHz, and the temperature was decreased from +10 to −30 °C. For the INEPT based experiments, the ^{1}H−^{13}C dephasing delay was set to 1.725 ms. All spectra were processed with 10 Hz of line broadening.

dx.doi.org/10.1021/bi401020t | Biochemistry 2013, 52, 7031−7040

water was monitored on the basis of the line width change of the ^{1}H chemical shift of the water signal. For a MAS frequency of 11 kHz, the freezing point of the solution was observed between nominal temperatures of −20 and −25 °C (Figure S9 of the Supporting Information). For the CP based experiments, the radio frequency fields on ^{1}H and ^{13}C channels were matched to the zero quantum condition (42 kHz on both channels), such that the Hartmann−Hahn condition for the CP transfer was nearly independent of the MAS frequency.[54] For the INEPT based methods, the $^{1}H-^{13}C$ dephasing delay was set to 1.725 ms ($1/4 \times J$) corresponding to the characteristic J_{CH} coupling constant of around 145 Hz. Cross-polarization relies on strong dipolar couplings, and is, therefore, an efficient transfer method for rigid samples, but not in solution where molecules undergo rapid reorientation with a correlation time $<10^{-5}$ s. On the other hand, regions with high mobility can be excited by INEPT magnetization transfer from protons to carbon.[55,56] In the case of NP7 at 10 °C, the presence of signals in both INEPT and CP spectra are indicative of the presence of both rigid and flexible moieties, which can, in principle be explained by the presence of monomers as well as by flexible parts within the aggregates (Figure 1, top left). A further decrease in temperature from +10 to −10 °C did not show significant influence in signal intensities for CP and INEPT based methods. However, the CP spectra recorded at −30 °C showed a drastic increase of CP signals by a factor of 4 in the absence and presence of MAS, due to the process of freezing within the temperature regime of −10 to −30 °C. The INEPT spectra of NP7 aggregates recorded at −30 °C were devoid of any signals from the protein indicating the absence of residual dynamics at this temperature.

Therefore, multidimensional ssNMR spectra based on CPMAS methods were performed at −30 °C. MAS at 11 kHz improved the spectral resolution significantly for both CPMAS and INEPTMAS, as anisotropic interactions were efficiently averaged out to yield well resolved resonance lines.

Figure 2 shows a plot of the relative intensities from Cα and CH_3 regions of one-dimensional ^{13}C CPMAS and INEPTMAS spectra of [U-^{13}C,^{15}N\(K,V)]NP7−NO aggregates as a function of temperature.

In the case of CPMAS, the Cα (55 ppm) regions from the protein backbone showed a 4-time increase in intensity at decreasing the nominal temperature from −10 to −30 °C. This effect is significant below −10 °C as indicated by dotted gray lines. In the case of INEPTMAS, the signal intensities from the Cα resonances showed a 4-time decrease in intensity below −10 °C, indicating that the mobility of the protein backbone is considerably reduced, and dissolved monomers were frozen in solution. To clarify whether the INEPT signals arise from either monomers present in the sample or from flexible parts of the aggregated proteins, we recorded a 2D $^{13}C-^{13}C$ INEPT-TOBSY[57−59] spectrum (Figure S5 of the Supporting Information). Cross peaks for all spin systems of all amino acid types could be identified; however, most cross peaks show chemical shifts typical for random coil conformation (Table S3 of the Supporting Information). Thus, we can conclude that these resonances are due to either unfolded monomers or flexible loop regions without defined secondary structure undergoing high amplitude fluctuations at time scales $<10^{-6}$ s. A 2D $^{13}C-^{13}C$ correlation spectrum recorded at a nominal temperature of 10 °C displays most interresidual cross peaks when the spin diffusion mixing time is as long as 100 ms (Figure S10 of the Supporting Information). However, as

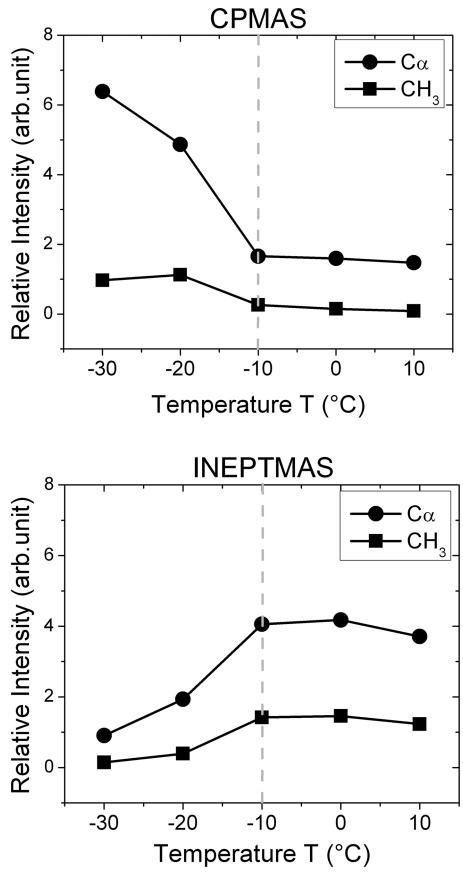

Figure 2. Relative signal intensities from representative regions of the 1D ^{13}C CPMAS and INEPTMAS spectra of [U-^{13}C,^{15}N\(K,V)]NP7−NO aggregates in the diamagnetic form plotted as a function of temperature. The representative regions correspond to the average chemical shifts for Cα (55 ppm) and Ile Cδ (14 ppm), respectively. The dotted gray lines at −10 °C indicate the process of freezing below this temperature.

dipolar transfer is more efficient at lower temperatures, we decided to record all spectra used for resonance assignment at a nominal temperature of −30 °C.

Resonance Assignments and Comparison to Data from X-ray Crystallography. For the diamagnetic sample, we could identify and assign residue-specific spin systems for 78 amino acids: 12 Ala, 2 Arg, 10 Asp/Asn, 1 Cys, 8 Glu/Gln, 9 Gly, 2 His, 5 Ile, 11 Phe/Tyr, 4 Pro, 6 Ser, and 8 Thr. Of these spin systems, we obtained site-specific assignments for 22 residues from a set of 2D $^{13}C-^{13}C$ (PDSD, DREAM, and SQ-DQ), 2D $^{15}N-^{13}C$ (NCA, NCO, NCACB, NCACX, and NCOCX), and 3D $^{15}N-^{13}C$ (NCACB, NCACX, and NCOCX) correlation spectra.

Amino acid type-specific intraresidual assignments were first established from a series of 2D $^{13}C-^{13}C$ and 2D and 3D $^{15}N-^{13}C$ (NCACB, NCACX) correlation spectra. An example for intraresidual NCACB correlations for two distinct Ala and one Thr residues is shown (Figure 3). 2D NCA and NCO spectra are shown in Figure S11 of the Supporting Information.

Inter-residual site-specific assignments were established by linking ^{15}N chemical shifts of the ith amino acid residue to the COCX of the previous residue (i − 1)th using 2D and 3D NCOCX spectra, along with the summary of the identified chemical shifts (Table S4 of the Supporting Information). Site-specific information was also obtained from inter-residual cross

dx.doi.org/10.1021/bi401020t | Biochemistry 2013, 52, 7031−7040

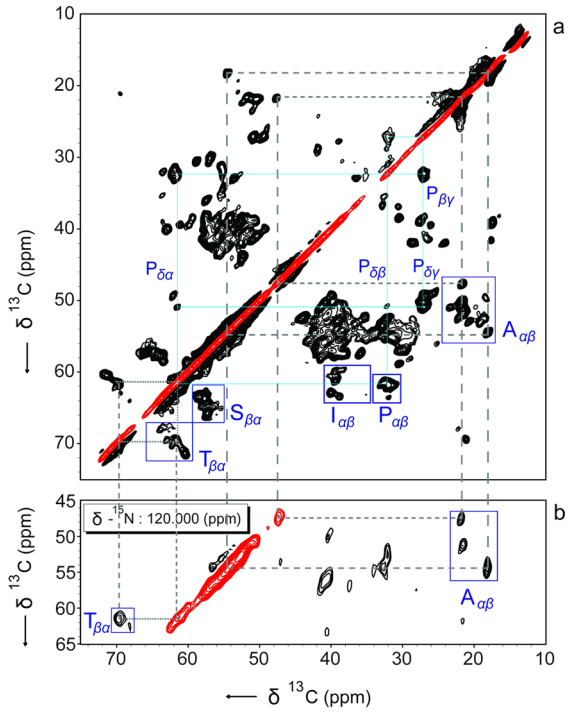

Figure 3. Aliphatic regions of (a) 2D ^{13}C−^{13}C DREAM and (b) 2D plane from 3D NCACB spectrum of [U-^{13}C,^{15}N\(K,V)]NP7−NO recorded using 15 kHz MAS and at −30 °C. The DREAM transfer during the mixing unit was set to 1.6 ms. Data were processed with a combination of an exponential and a Gaussian function (−150 Hz exponential, Gaussian factor 0.2). Fingerprint regions from Ala, Ile, Pro, Ser, and Thr are shown in blue rectangles with intraresidual assignments for the Ala and Thr residues shown with dotted gray lines. Side chain walk for the Pro residue is shown by colored lines (cyan).

peaks in spin diffusion spectra recorded at longer spin diffusion mixing times under weak coupling conditions[60] (100 ms) (Figures S12−S14 of the Supporting Information).

Our resonance assignments agree reasonably well with the preliminary X-ray crystal structure of NP7 (resolution 1.8 Å)[19] (Figure 4a). NP7 contains a β-barrel made up of eight antiparallel β-strands A to H consisting of 69 residues in total, and two main α-helices (α1, α2) in the C-terminus comprising 16 residues. Secondary chemical shifts of the site-specifically assigned residues based on CPMAS spectra show predominantly β-strand character (Figure 5b). Previous reports on other nitrophorins (NP1−4) have revealed that eight β-strands are the best ordered in the structure while the connecting loops showed high flexibility.[32,61−71] A comparison of the 2D ^{13}C−^{13}C DREAM spectrum with the chemical shifts predicted by SHIFTX2[72] with the preliminary X-ray structure are in good agreement (Figure S5 of the Supporting Information). This indicates that even though we are looking at insoluble precipitates, the native fold of the protein is well preserved.

Pseudocontact Shifts. Depending on the ligand bound to the heme center, NP7 can adopt different electronic spin states. Figure 5 displays a superposition of the aliphatic regions of the 2D ^{13}C−^{13}C DREAM[73] spectra of LS [U-^{13}C,^{15}N\(K,V)]NP7−ImH (black) and diamagnetic [U-^{13}C,^{15}N\(K,V)]NP7−NO (red).

The spectra obtained from both electronic spin states are well resolved and almost identical. However, minor differences can be detected for some resonances in the 2D ^{13}C−^{13}C DREAM spectra.[74−77] For example, high frequency shifts of 0.8

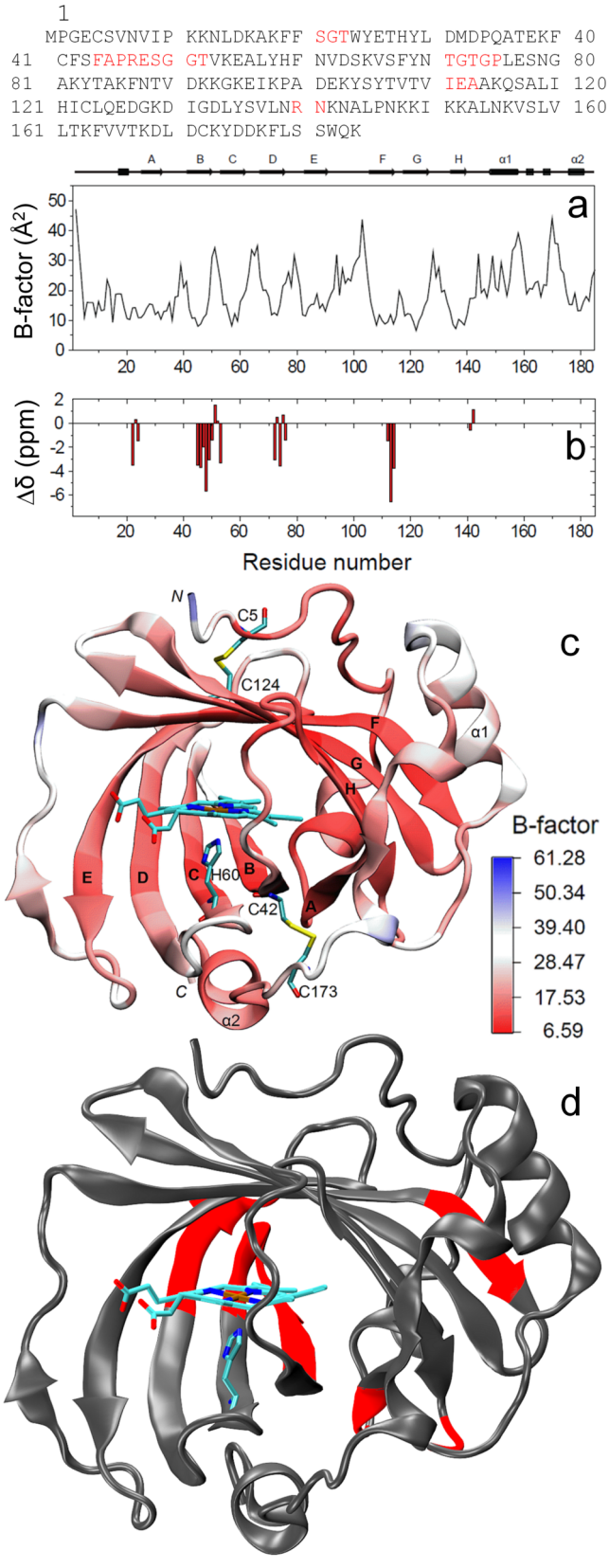

Figure 4. X-ray crystallographic *B*-factor values of backbone Cα atoms along NP7 residues. Schematic representation of the NP7 secondary structure based on STRIDE secondary structure analysis is displayed on the top. (b) ^{13}C secondary chemical shifts of NP7 based on site-specific sequential assignments. The secondary chemical shifts based on sequential assignments are calculated as, $\Delta C\alpha$ = Cα(Experimental) − Cα(BMRB) and $\Delta C\beta$ = Cβ(Experimental) − Cβ(BMRB). (c)

dx.doi.org/10.1021/bi401020t | *Biochemistry* 2013, 52, 7031−7040

Figure 4. continued

Modified cartoon representation of NP7 crystal structure. The coloring scheme is based on the X-ray crystallographic *B*-factor values. The main β-strands are designated from A to H in bold letters along with two main α-helices. The N- and C-termini are designated with italic letters. The four disulfide-forming Cys residues, the heme cofactor, and the proximal His-60 are displayed in the "liquorice" style. Figure 4c was rendered with visual molecular dynamics (VMD). (d) Similar representation as (c). The red regions represent the areas where the residues have been assigned (see Table S4 of the Supporting Information).

and 3.2 ppm for Cβ resonances of two Ile residues are observed in the spectrum of the LS form (Figure 5c). PCSs can be approximated[22,78] from the main values of the *g*-tensor,[9] the orientation of the *g*-tensor within the molecular frame[79] and with respect to the heme group and the X-ray crystal structure.[19] For a nucleus at a distance of 12 Å from the electron spin, the PCS will range between +1.3 and −1.0 ppm, and for a nucleus at a distance of 6.8 Å between 7.9 and −6.7 ppm. In total, three Ile residues (Ile121, Ile123, and Ile132) are in close enough proximity to the heme center to explain these shift differences. The *z*-axis of the *g*-tensor was found close to perpendicular to the heme plane. For Ile123 and Ile132, positive PCS can be expected (see Supporting Information), whereas for Ile121, the PCS should be negative. Thus, the two positively shifted cross peaks may be tentatively assigned to Ile123 and Ile132. Negative PCS could, however, not be observed, which may be due to signal overlap. Another possible explanation for the observed changes of chemical shifts dependent on the distal heme ligand that should be considered is a conformational change of certain side chains and/or a change of the chemical environment, for example, by change of the polarity in the distal heme pocket. Ile123 forms part of the distal heme pocket and is thus in close proximity to the ligand (Ile123:Cβ↔Fe ≈ 7 Å). Therefore, a contribution of the ligand to the change in chemical shifts cannot be ruled out. However, the other two residues are located in much larger distance from the distal heme ligand (Cβ↔Fe ≈ 11 Å) and cannot be directly influenced by the distal pocket heme ligand. A large structural rearrangement in the protein induced by the distal heme ligand that affects the long distance residues from the heme pocket is not supported by any known data including the spectra recorded herein. Therefore, although a contribution of the ligand type on the chemical shifts of the three Ile residues cannot be completely ruled out, the PCS through-space effect seems more likely for the chemical shifts observed.

CONCLUSION

The development of the expression and purification protocol of the heme protein NP7 in the isotopically labeled form [U-^{13}C,^{15}N\(K,V)]NP7 enabled us to record ssNMR spectra of precipitated NP7. For today's development of ssNMR spectroscopy, the size of the protein (21 kDa) still poses a challenge for full structural determination. Thus, the reverse labeling of some of the most abundant amino acid residues significantly simplified the spectrum. For the less frequent amino acids in the NP7 sequence (Met and Trp), complete spin system identification was not yet possible due to spectral overlap. Furthermore, the use of the two electronic spin states $S = 0$ and $S = 1/2$ of the ferriheme allowed the identification of two residues due to paramagnetic shifting induced through PCS, which is demonstrated here for the proximal heme pocket residues Ile123 and Ile132. An important outcome of the ssNMR study is the detailed investigation of the NP7 oligomerization state, which was previously reported, but the effects on the structure could not be predicted. It is clear now that at concentrations of approximately 0.1−2 mM oligomers are in equilibrium with monomers. Furthermore, the protein oligomerizes preferably in units of trimers, hexamers, and higher oligomeric states of unidentified composition. However, the fact that well-folded monomers are not visible in the

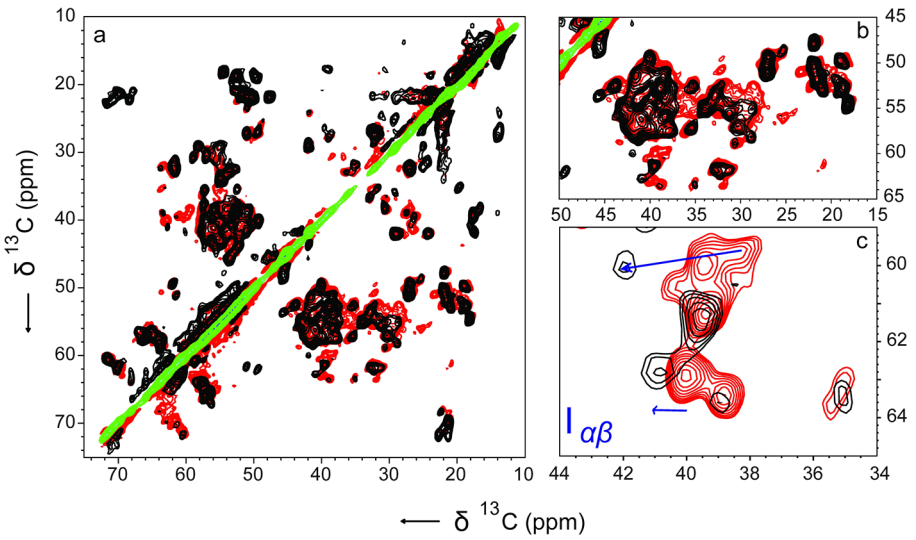

Figure 5. Superposition of aliphatic region of 2D ^{13}C−^{13}C DREAM correlation spectra of [U-^{13}C,^{15}N\(K,V)]NP7−ImH (black) [U-^{13}C,^{15}N\(K,V)]NP7−NO (red) recorded using a MAS frequency of 15 kHz and at −30 °C. The selected regions of the same spectra correspond to (b) aliphatic Cα-Cβ and (c) Ile Cα-Cβ. The DREAM transfer during the mixing unit was set to 1.6 ms. The other acquisition parameters were 0.3 ms ^{1}H−^{13}C CP contact time, 83 kHz ^{1}H SPINAL decoupling, 5 ms acquisition time in the indirect dimension with States detection, 13 ms acquisition time in the direct dimension, and 2 s recycle delay. The data were processed with a combination of an exponential and a Gaussian function (−150 Hz exponential, Gaussian factor 0.2) and zero filled to 512 (F2) × 4096 (F1) complex points.

dx.doi.org/10.1021/bi401020t | *Biochemistry* 2013, 52, 7031−7040

INEPT-TOBSY spectra demonstrates that at concentrations required for ssNMR (>2 mM) oligomers form a precipitate that does not dissolve into monomers again. The total concentration of NPs in the saliva of *R. prolixus* is indeed very high, reaching millimolar concentration.[80] However, data about the particular salivary concentration of NP7 are currently not available, so that it is possible that NP7 appears in the saliva in oligomerized form.

More importantly, the current study provides a solid basis for future investigations by ssNMR studies, which, together with the crystallographic progress, will help to understand this novel isoform among the nitrophorins. The protein is of major importance among the nitrophorins because it is the only isoform that binds to phospholipid membranes. Moreover, the translocation of NO across cell membranes is a major and important event in NO signaling. Consequently, other heme proteins involved with NO signaling, such as endothelial nitric oxide synthase (eNOS)[81] or the $\beta 2$ homodimer of soluble guanylate cyclase ($(\beta 2)_2$sGC),[82] are located at the phospholipid membrane surface. However, the structural examination of the membrane bound forms of such proteins by NMR is rather difficult due to their sheer size. In contrast, NP7 presents the smallest example of a membrane attaching heme protein involved in NO signaling and is, therefore, an important target to be studied in detail to elucidate the structure function relationships involved with membrane attaching. Very recently, a series of three interconnected gas hosting cavities was established by molecular dynamics simulation.[83] Interestingly, this tunnel reaches from the heme pocket through the back part of the protein toward the membrane attaching surface suggesting some functional role for NO delivery. Thus, the data presented herein demonstrate that ssNMR will allow us to focus particularly on the important structural consequences of the NP7-membrane interaction, which cannot be assessed by solution NMR or X-ray crystallography. In addition, ssNMR spectroscopy will allow to study the dynamics of NP7 which then, in combination with X-ray crystallography, spectroscopic, and computational methods provides insight into the function of this very unique example of a membrane attaching NO transporter.

■ ASSOCIATED CONTENT

Supporting Information

Elution profiles of NP7 bo und to Ca^{2+} charged Chelating Sepharose HP monitored by the absorbance at 280 nm, Coomassie stained SDS−PAGE, MALDI Q-TOF MS spectra, NP7 visual observations, overlays of the aliphatic regions, data fitting of T_1 and T_2 measurements of a hyperfine-shifted resonance in the downfield region of 2 mM NP2-ImH and NP7−ImH, 2D DOSY NMR plots, 1D ^{1}H spectra, correlation spectra of [U-^{13}C,^{15}N\(K,V)]NP7−NO, chemical shift assignments of R48 and R141, strip plot showing the sequential assignments from T53 to S50, selected regions of the 2D ^{13}C−^{13}C PDSD spectra of [U-^{13}C,^{15}N\(K,V)]NP7−NO, molecular masses of the various NP7 isotope labeling states, a description of the estimation of the pseudocontact shifts, and distance measurements of Ile residues. This material is available free of charge via the Internet at http://pubs.acs.org.

■ AUTHOR INFORMATION

Corresponding Authors

*PD Dr. Markus Knipp. E-mail: markus.knipp@cec.mpg.de. Tel.: +49-208-3063671.

*Prof. Dr. H. Heise, E-mail: h.heise@fz-juelich.de. Tel.: +49-2461-614658.

Author Contributions

The manuscript was written through contributions of all authors. All authors have given approval to the final version of the manuscript.

Funding

This work was supported in part by the Max Planck Society (MPG) (to M. K.) and the Entrepreneur Foundation at the Heinrich-Heine-University of Düsseldorf (to H. H.).

Notes

The authors declare no competing financial interest.

■ ACKNOWLEDGMENTS

The authors thank Johanna J. Taing and Norbert Dickmann for technical assistance and Dr. Oliver Bannach for recording the micrograph. We are grateful to Prof. F. Ann Walker, Department of Chemistry and Biochemistry, University of Tucson, AZ, for the allowing us to carry out the T_1 and T_2 relaxation experiments in her lab and for the helpful discussions.

■ ABBREVIATIONS

CP, cross-polarization; CPMAS, cross-polarization magic-angle spinning; CPMG, Carr−Purcell−Meiboom−Gill pulse sequence; DEA/NO, diethylammonium (*Z*)-1-(*N*,*N*-diethylamino)diazenolate-2-oxide; DLS, dynamic light scattering; DOSY, diffusion ordered spectroscopy; DREAM, dipolar recoupling enhancement by amplitude modulation; HSQC, heteronuclear single quantum correlation; ImH, imidazole; INEPT, insensitive nuclei enhanced by polarization transfer; MALDI MS, matrix-assisted laser desorption/ionization mass spectrometry; MAS, magic-angle spinning; PCS, pseudocontact shift; PC/PS, phosphatidyl choline/phosphatidyl serine; PRE, paramagnetic relaxation enhancement; PDSD, proton driven spin diffusion; SPINAL, small phase incremental alteration; SQ-DQ, single quantum double quantum; ssNMR, solid-state nuclear magnetic resonance; TOBSY, through bond correlation spectroscopy; [U-^{13}C,^{15}N\(K,V)]NP7, ^{13}C and ^{15}N labeled NP7 with Lys and Val in natural abundance

■ REFERENCES

(1) Knipp, M., and He, C. (2012) Nitrophorins: Nitrite disproportionation reaction and other novel functionalities of insect heme-based nitric oxide transport proteins. *IUBMB Life 63*, 304−312.

(2) Soares, A. C., Carvalho-Tavares, J., Gontijo, N. d. F., dos Santos, V. n. C., Teixeira, M. M., and Pereira, M. H. c. (2006) Salivation pattern of Rhodnius prolixus (Reduviidae; Triatominae) in mouse skin. *J. Insect Physiol. 52*, 468−472.

(3) Lehane, J. (2005) The Biology of Blood-Sucking in Insects, Cambridge University Press, Cambridge, U.K.

(4) Ignarro, L. J. (1990) Biosynthesis and metabolism of endothelium-derived nitric-oxide. *Annu. Rev. Pharmacol. Toxicol. 30*, 535−560.

(5) Bredt, D. S., and Snyder, S. H. (1994) Nitric Oxide: A Physiologic Messenger Molecule. *Annu. Rev. Biochem. 63*, 175−195.

(6) Montfort, W. R., Weichsel, A., and Andersen, J. F. (2000) Nitrophorins and related antihemostatic lipocalins from Rhodnius prolixus and other blood-sucking arthropods. *Biochim. Biophys. Acta, Protein Struct. Mol. Enzymol. 1482*, 110−118.

(7) Ribeiro, J. M. C., Hazzard, J. M. H., Nussenzveig, R. H., Champagne, D. E., and Walker, F. A. (1993) Reversible binding of nitric oxide by a salivary heme protein by a bloodsucking insect. *Science 260*, 539−541.

(8) Andersen, J. F., Gudderra, N. P., Francischetti, I. M. B., Valenzuela, J. G., and Ribeiro, J. M. C. (2004) Recognition of Anionic Phospholipid Membranes by an Antihemostatic Protein from a Blood-Feeding Insect. *Biochemistry 43*, 6987−6994.
(9) Knipp, M., Yang, F., Berry, R. E., Zhang, H., Shokhirev, M. N., and Walker, F. A. (2007) Spectroscopic and Functional Characterization of Nitrophorin 7 from the Blood-Feeding Insect Rhodnius prolixus Reveals an Important Role of Its Isoform-Specific N-Terminus for Proper Protein Function. *Biochemistry 46*, 13254−13268.
(10) Knipp, M., Zhang, H., Berry, R. E., and Walker, F. A. (2007) Overexpression in Escherichia coli and functional reconstitution of the liposome binding ferriheme protein nitrophorin 7 from the blood-sucking bug Rhodnius prolixus. *Protein Expression Purif. 54*, 183−191.
(11) Knipp, M., Soares, R. P., and Pereira, M. H. (2012) Identification of the native N-terminus of the membrane attaching ferriheme protein nitrophorin 7 from Rhodnius prolixus. *Anal. Biochem. 424*, 79−81.
(12) Shokhireva, T. K., Berry, R. E., Uno, E., Balfour, C. A., Zhang, H., and Walker, F. A. (2003) Electrochemical and NMR spectroscopic studies of distal pocket mutants of nitrophorin 2: Stability, structure, and dynamics of axial ligand complexes. *Proc. Natl. Acad. Sci. U. S. A. 100*, 3778−3783.
(13) Shokhireva, T. K., Shokhirev, N. V., and Walker, F. A. (2003) Assignment of heme resonances and determination of the electronic structures of high- and low-spin nitrophorin 2 by ^{1}H and ^{13}C NMR spectroscopy: An explanation of the order of heme methyl resonances in high-spin ferriheme proteins. *Biochemistry 42*, 679−693.
(14) Shokhireva, T. K., Smith, K. M., Berry, R. E., Shokhirev, N. V., Balfour, C. A., Zhang, H., and Walker, F. A. (2007) Assignment of the ferriheme resonances of the high-spin forms of nitrophorins 1 and 4 by ^{1}H NMR spectroscopy: Comparison to structural data obtained from X-ray crystallography. *Inorg. Chem. 46*, 170−178.
(15) Shokhireva, T. K., Weichsel, A., Smith, K. M., Berry, R. E., Shokhirev, N. V., Balfour, C. A., Zhang, H., Montfort, W. R., and Walker, F. A. (2007) Assignment of the ferriheme resonances of the low-spin complexes of nitrophorins 1 and 4 by ^{1}H and ^{13}C NMR spectroscopy: Comparison to structural data obtained from X-ray crystallography. *Inorg. Chem. 46*, 2041−2056.
(16) Shokhireva, T. K., Berry, R. E., Zhang, H., Shokhirev, M. N., and Walker, F. A. (2008) Assignment of ferriheme resonances for high- and low-spin forms of nitrophorin 3 by ^{1}H and ^{13}C NMR spectroscopy and comparison to nitrophorin 2: Heme pocket structural similarities and differences. *Inorg. Chim. Acta 361*, 925−940.
(17) Yang, F., Knipp, M., Shokhireva, T. K., Berry, R. E., Zhang, H., and Walker, F. A. (2009) ^{1}H and ^{13}C NMR spectroscopic studies of the ferriheme resonances of three low-spin complexes of wild-type nitrophorin 2 and nitrophorin 2(V24E) as a function of pH. *JBIC, J. Biol. Inorg. Chem. 14*, 1077−1095.
(18) Yang, F., Zhang, H., and Knipp, M. (2008) A One-Residue Switch Reverses the Orientation of a Heme b Cofactor. Investigations of the Ferriheme NO Transporters Nitrophorin 2 and 7 from the Blood-Feeding Insect Rhodnius prolixus. *Biochemistry 48*, 235−241.
(19) Ogata, H., and Knipp, M. (2012) Crystallization and preliminary X-ray crystallographic analysis of the membrane-binding haemprotein nitrophorin 7 from Rhodnius prolixus. *Acta Crystallogr. Sect. F: Struct. Biol. Cryst. Commun. 68*, 37−40.
(20) (2013) Special Issue "Frontiers in Solid State NMR Technology ", *Acc. Chem. Res., 46* (9).
(21) Jaroniec, C. P. (2012) Solid-state nuclear magnetic resonance structural studies of proteins using paramagnetic probes. *Solid State Nucl. Magn. Reson. 43*−*44*, 1−13.
(22) Bertini, I., Luchinat, C., and Parigi, G. (2001) *Solution NMR of paramagnetic molecules applications to metallobiomolecules and models*, Elsevier Science Ltd., Amsterdam; New York.
(23) Pintacuda, G., and Kervern, G. (2013) Paramagnetic Solid-State Magic-Angle Spinning NMR Spectroscopy, in *Modern NMR Methodology* (Heise, H., and Matthews, S., Eds.), pp 157−200, Springer, Berlin; Heidelberg.
(24) Jovanovic, T., Farid, R., Friesner, R. A., and McDermott, A. E. (2005) Thermal equilibrium of high- and low-spin forms of cytochrome P450BM-3: Repositioning of the substrate? *J. Am. Chem. Soc. 127*, 13548−13552.
(25) Jovanovic, T., and McDermott, A. E. (2005) Observation of Ligand Binding to Cytochrome P450 BM-3 by Means of Solid-State NMR Spectroscopy. *J. Am. Chem. Soc. 127*, 13816−13821.
(26) Balayssac, S., Bertini, I., Fälber, K., Fragai, M., Jehle, S., Lelli, M., Luchinat, C., Oschkinat, H., and Yeo, K. J. (2007) Solid-State NMR of Matrix Metalloproteinase 12: An Approach Complementary to Solution NMR. *ChemBioChem 8*, 486−489.
(27) Balayssac, S., Bertini, I., Lelli, M., Luchinat, C., and Maletta, M. (2007) Paramagnetic Ions Provide Structural Restraints in Solid-State NMR of Proteins. *J. Am. Chem. Soc. 129*, 2218−2219.
(28) Balayssac, S., Bertini, I., Bhaumik, A., Lelli, M., and Luchinat, C. (2008) Paramagnetic shifts in solid-state NMR of proteins to elicit structural information. *Proc. Nat. Acad. Sci. U. S. A. 105*, 17284−17289.
(29) Luchinat, C., Parigi, G., Ravera, E., and Rinaldelli, M. (2012) Solid-State NMR Crystallography through Paramagnetic Restraints. *J. Am. Chem. Soc. 134*, 5006−5009.
(30) Knight, M. J., Pell, A. J., Bertini, I., Felli, I. C., Gonnelli, L., Pierattelli, R., Herrmann, T., Emsley, L., and Pintacuda, G. (2012) Structure and backbone dynamics of a microcrystalline metalloprotein by solid-state NMR. *Proc. Natl. Acad. Sci. U. S. A. 109*, 11095−11100.
(31) Enemark, J. H., and Feltham, R. D. (1974) Principles of structure, bonding, and reactivity for metal nitrosyl complexes. *Coord. Chem. Rev. 13*, 339−406.
(32) Andersen, J. F., Weichsel, A., Balfour, C. A., Champagne, D. E., and Montfort, W. R. (1998) The crystal structure of nitrophorin 4 at 1.5 Å resolution: transport of nitric oxide by a lipocalin-based heme protein. *Structure 6*, 1315−1327.
(33) Brand, T., Cabrita, E. J., Morris, G. A., Günther, R., Hofmann, H.-J., and Berger, S. (2007) Residue-specific NH exchange rates studied by NMR diffusion experiments. *J. Magn. Reson. 187*, 97−104.
(34) Wu, D. H., Chen, A. D., and Johnson, C. S. (1995) An Improved Diffusion-Ordered Spectroscopy Experiment Incorporating Bipolar-Gradient Pulses. *J. Magn. Reson., Ser. A 115*, 260−264.
(35) Price, W. S. (1998) Pulsed-field gradient nuclear magnetic resonance as a tool for studying translational diffusion: Part II. Experimental aspects. *Concepts Magn. Reson. 10*, 197−237.
(36) Antalek, B. (2002) Using pulsed gradient spin echo NMR for chemical mixture analysis: How to obtain optimum results. *Concepts Magn. Reson. 14*, 225−258.
(37) Price, W. S., Elwinger, F., Vigouroux, C., and Stilbs, P. (2002) PGSE-WATERGATE, a new tool for NMR diffusion-based studies of ligand−macromolecule binding. *Magn. Reson. Chem. 40*, 391−395.
(38) Price, W. S. (1997) Pulsed-field gradient nuclear magnetic resonance as a tool for studying translational diffusion: Part 1. Basic theory. *Concepts Magn. Reson. 9*, 299−336.
(39) Brand, T., Cabrita, E. J., Berger, S., and Webb, G. A. (2006) Theory and Application of NMR Diffusion Studies. *Mod. Magn. Reson.*, pp 135−143, Springer, The Netherlands.
(40) Pines, A., Gibby, M. G., and Waugh, J. S. (1973) Proton-enhanced NMR of dilute spins in solids. *J. Chem. Phys. 59*, 569−590.
(41) Fung, B. M., Khitrin, A. K., and Ermolaev, K. (2000) An improved broadband decoupling sequence for liquid crystals and solids. *J. Magn. Reson. 142*, 97−101.
(42) Delaglio, F., Grzesiek, S., Vuister, G. W., Zhu, G., Pfeifer, J., and Bax, A. (1995) NMRpipe - a multidimensional spectral processing system based on unix pipes. *J. Biomol. NMR 6*, 277−293.
(43) Morcombe, C. R., and Zilm, K. W. (2003) Chemical shift referencing in MAS solid state NMR. *J. Magn. Reson. 162*, 479−486.
(44) Heise, H., Köhler, F. H., and Xie, X. (2001) Solid-State NMR Spectroscopy of Paramagnetic Metallocenes. *J. Magn. Reson. 150*, 198−206.
(45) Heise, H., Hoyer, W., Becker, S., Andronesi, O. C., Riedel, D., and Baldus, M. (2005) Molecular-level secondary structure, polymorphism, and dynamics of full-length alpha-synuclein fibrils studied by solid-state NMR. *Proc. Natl. Acad. Sci. U. S. A. 102*, 15871−15876.

(46) Waugh, D. S. (1996) Genetic tools for selective labeling of proteins with alpha-N-15-amino acids. *J. Biomol. NMR 8*, 184−192.
(47) Johnson, C. S., Jr. (1999) Diffusion ordered nuclear magnetic resonance spectroscopy: principles and applications. *Prog. Nucl. Magn. Reson. Spectrosc. 34*, 203−256.
(48) Jerschow, A., and Müller, N. (1997) Suppression of Convection Artifacts in Stimulated-Echo Diffusion Experiments. Double-Stimulated-Echo Experiments. *J. Magn. Reson. 125*, 372−375.
(49) Hua, Q.-x., Dementieva, I. S., Walsh, M. A., Hallenga, K., Weiss, M. A., and Joachimiak, A. (2001) A thermophilic mini-chaperonin contains a conserved polypeptide-binding surface: combined crystallographic and NMR studies of the GroEL apical domain with implications for substrate interactions. *J. Mol. Biol. 306*, 513−525.
(50) Sprangers, R., and Kay, L. E. (2007) Quantitative dynamics and binding studies of the 20S proteasome by NMR. *Nature 445*, 618−622.
(51) Hartmann, S. R., and Hahn, E. L. (1962) Nuclear Double Resonance in the Rotating Frame. *Phys. Rev. 128*, 2042−2053.
(52) Morris, G. A., and Freeman, R. (1979) Enhancement of nuclear magnetic resonance signals by polarization transfer. *J. Am. Chem. Soc. 101*, 760−762.
(53) Bertini, I., Luchinat, C., Parigi, G., Ravera, E., Reif, B., and Turano, P. (2011) Solid-state NMR of proteins sedimented by ultracentrifugation. *Proc. Nat. Acad. Sci. U. S. A. 108*, 10396−10399.
(54) Stejskal, E. O., Schaefer, J., and Waugh, J. S. (1977) Magic-angle spinning and polarization transfer in proton-enhanced NMR. *J. Magn. Reson. 28*, 105−112.
(55) Andronesi, O. C., Becker, S., Seidel, K., Heise, H., Young, H. S., and Baldus, M. (2005) Determination of membrane protein structure and dynamics by magic-angle-spinning solid-state NMR spectroscopy. *J. Am. Chem. Soc. 127*, 12965−12974.
(56) Siemer, A. B., Arnold, A. A., Ritter, C., Westfeld, T., Ernst, M., Riek, R., and Meier, B. H. (2006) Observation of highly flexible residues in amyloid fibrils of the HET-s prion. *J. Am. Chem. Soc. 128*, 13224−13228.
(57) Baldus, M., and Meier, B. H. (1996) Total Correlation Spectroscopy in the Solid State. The Use of Scalar Couplings to Determine the Through-Bond Connectivity. *J. Magn. Reson., Ser. A 121*, 65−69.
(58) Baldus, M., Iuliucci, R. J., and Meier, B. H. (1997) Probing through-bond connectivities and through-space distances in solids by magic-angle-spinning nuclear magnetic resonance. *J. Am. Chem. Soc. 119*, 1121−1124.
(59) Hardy, E. H., Verel, R., and Meier, B. H. (2001) Fast MAS Total Through-Bond Correlation Spectroscopy. *J. Magn. Reson. 148*, 459−464.
(60) Seidel, K., Lange, A., Becker, S., Hughes, C. E., Heise, H., and Baldus, M. (2004) Protein solid-state NMR resonance assignments from (C-13, C-13) correlation spectroscopy. *Phys. Chem. Chem. Phys. 6*, 5090−5093.
(61) Amoia, A. M., and Montfort, W. R. (2007) Apo-nitrophorin 4 at atomic resolution. *Protein Sci. 16*, 2076−2081.
(62) Abbruzzetti, S., He, C., Ogata, H., Bruno, S., Viappiani, C., and Knipp, M. (2012) Heterogeneous Kinetics of the Carbon Monoxide Association and Dissociation Reaction to Nitrophorin 4 and 7 Coincide with Structural Heterogeneity of the Gate-Loop. *J. Am. Chem. Soc. 134*, 9986−9998.
(63) Roberts, S. A., Weichsel, A., Qiu, Y., Shelnutt, J. A., Walker, F. A., and Montfort, W. R. (2001) Ligand-Induced Heme Ruffling and Bent NO Geometry in Ultra-High-Resolution Structures of Nitrophorin 4. *Biochemistry 40*, 11327−11337.
(64) Weichsel, A., Andersen, J. F., Roberts, S. A., and Montfort, W. R. (2000) Nitric oxide binding to nitrophorin 4 induces complete distal pocket burial. *Nat. Struct. Biol. 7*, 551−554.
(65) Kondrashov, D. A., Roberts, S. A., Weichsel, A., and Montfort, W. R. (2004) Protein Functional Cycle Viewed at Atomic Resolution: Conformational Change and Mobility in Nitrophorin 4 as a Function of pH and NO Binding. *Biochemistry 43*, 13637−13647.
(66) Maes, E. M., Weichsel, A., Andersen, J. F., Shepley, D., and Montfort, W. R. (2004) Role of Binding Site Loops in Controlling Nitric Oxide Release: Structure and Kinetics of Mutant Forms of Nitrophorin 4. *Biochemistry 43*, 6679−6690.
(67) Nienhaus, K., Maes, E. M., Weichsel, A., Montfort, W. R., and Nienhaus, G. U. (2004) Structural Dynamics Controls Nitric Oxide Affinity in Nitrophorin 4. *J. Biol. Chem. 279*, 39401−39407.
(68) Benabbas, A., Ye, X., Kubo, M., Zhang, Z., Maes, E. M., Montfort, W. R., and Champion, P. M. (2010) Ultrafast Dynamics of Diatomic Ligand Binding to Nitrophorin 4. *J. Am. Chem. Soc. 132*, 2811−2820.
(69) Maes, E. M., Roberts, S. A., Weichsel, A., and Montfort, W. R. (2005) Ultrahigh Resolution Structures of Nitrophorin 4: Heme Distortion in Ferrous CO and NO Complexes. *Biochemistry 44*, 12690−12699.
(70) Andersen, J. F., and Montfort, W. R. (2000) The Crystal Structure of Nitrophorin 2. *J. Biol. Chem. 275*, 30496−30503.
(71) Berry, R. E., Shokhireva, T. K., Filippov, I., Shokhirev, M. N., Zhang, H., and Walker, F. A. (2007) Effect of the N-Terminus on Heme Cavity Structure, Ligand Equilibrium, Rate Constants, and Reduction Potentials of Nitrophorin 2 from Rhodnius prolixus. *Biochemistry 46*, 6830−6843.
(72) Han, B., Liu, Y., Ginzinger, S., and Wishart, D. (2011) SHIFTX2: significantly improved protein chemical shift prediction. *J. Biomol. NMR 50*, 43−57.
(73) Verel, R., Ernst, M., and Meier, B. H. (2001) Adiabatic dipolar recoupling in solid-state NMR: The DREAM scheme. *J. Magn. Reson. 150*, 81−99.
(74) Bertini, I., Luchinat, C., and Parigi, G. (2002) Paramagnetic constraints: An aid for quick solution structure determination of paramagnetic metalloproteins. *Concepts Magn. Reson. 14*, 259−286.
(75) Pintacuda, G., John, M., Su, X.-C., and Otting, G. (2007) NMR Structure Determination of Protein-Ligand Complexes by Lanthanide Labeling. *Acc. Chem. Res. 40*, 206−212.
(76) Mayo, B. C. (1973) Lanthanide shift reagents in nuclear magnetic resonance spectroscopy. *Chem. Soc. Rev. 2*, 49−74.
(77) Harden, M. M., and Richard, E. R. (1958) Isotropic Nuclear Resonance Shifts. *J. Chem. Phys. 29*, 1361−1365.
(78) Kurland, R. J., and McGarvey, B. R. (1970) Isotropic NMR shifts in transition metal complexes: The calculation of the fermi contact and pseudocontact terms. *J. Magn. Reson. 2*, 286−301.
(79) Astashkin, A. V., Raitsimring, A. M., and Walker, F. A. (1999) Two- and four-pulse ESEEM studies of the heme binding center of a low-spin ferriheme protein: the importance of a multi-frequency approach. *Chem. Phys. Lett. 306*, 9−17.
(80) Ribeiro, J. M. C., and Garcia, E. S. (1981) Platelet anti-aggregating activity in the salivary secretion of the blood-sucking bug rhodnius prolixus. *Experientia 37*, 384−386.
(81) Shaul, P. W. (2002) Regulation of endothelial nitric oxide synthase: Location, location, location. *Annu. Rev. Physiol. 64*, 749−774.
(82) Derbyshire, E. R., and Marletta, M. A. (2012) Structure and Regulation of Soluble Guanylate Cyclase. *Annu. Rev. Biochem. 81*, 533−559.
(83) Oliveira, A., Allegri, A., Bidon-Chanal, A., Knipp, M., Roitberg, A. E., Abbruzzetti, S., Viappiani, C., and Luque, F. J. (2013) Kinetics and computational studies of ligand migration in nitrophorin 7 and its Δ1−3 mutant. *Biochim. Biophys. Acta, Proteins Proteomics 1834*, 1711−1721.